Magn Reson Med Sci 2018; 17; 73–79
doi:10.2463/mrms.mp.2016-0145 Published Online: May 18, 2017

MAJOR PAPER

Magnetic Susceptibility Changes in the Basal Ganglia and Brain Stem of Patients with Wilson's Disease: Evaluation with Quantitative Susceptibility Mapping

Selim Doganay[1], Kazim Gumus[2*], Gonca Koc[1], Ayse Kacar Bayram[3], Mehmet Sait Dogan[1], Duran Arslan[4], Hakan Gumus[3], Sureyya Burcu Gorkem[1], Saliha Ciraci[1], Halil Ibrahim Serin[5], and Abdulhakim Coskun[1]

Objectives: Wilson's disease (WD) is characterized with the accumulation of copper in the liver and brain. The objective of this study is to quantitatively measure the susceptibility changes of basal ganglia and brain stem of pediatric patients with neurological WD using quantitative susceptibility mapping (QSM) in comparison to healthy controls.

Methods: Eleven patients with neurological WD (mean age 15 ± 3.3 years, range 10–22 years) and 14 age-matched controls were prospectively recruited. Both groups were scanned on a 1.5 Tesla clinical scanner. In addition to T_1- and T_2-weighted MR images, a 3D multi-echo spoiled gradient echo (GRE) sequence was acquired and QSM images were derived offline. The quantitative measurement of susceptibility of corpus striatum, thalamus of each hemisphere, midbrain, and pons were assessed with the region of interest analysis on the QSM images. The susceptibility values for the patient and control groups were compared using two-sample *t*-test.

Results: One patient with WD had T_1 shortening in the bilateral globus pallidus. Another one had hyperintensity in the bilateral putamen, caudate nuclei, and substantia nigra on T_2-weighted images. The rest of the patients with WD and all subjects of the control group had no signal abnormalities on conventional MR images. The susceptibility measures of right side of globus pallidus, putamen, thalamus, midbrain, and entire pons were significantly different in patients compared to controls ($P < 0.05$).

Conclusion: QSM method exhibits increased susceptibility differences of basal ganglia and brain stem in patients with WD that have neurologic impairment even if no signal alteration is detected on T_1- and T_2-weighted MR images.

Keywords: *quantitative susceptibility mapping, magnetic resonance imaging, Wilson's disease, copper*

Introduction

Wilson's Disease (WD) is an inherited copper metabolism disorder resulted from a mutation to *ATP7B* gene acting in the transportation of the copper.[1] Due to defective transportation, copper accumulates particularly in the liver and brain. This is assumed to be the main mechanism responsible for the pathogenesis of the disease.[2–4] Thus, the spectrum of clinical presentations consists of hepatic, neurological, or neuropsychiatric disturbances. Main neurological symptoms associated with WD include dizziness, lack of strength, excessive salivation, slurred speech, ataxia, dystonia, bradykinesia, personality changes, and headache. The diagnosis of clinically suspected patients is based on the combinations of the presence of Kayser-Fleischer ring detected by slit lamp examination, decreased level of serum ceruloplasmin, increased excretion of urinary copper, and eventually detection of excessive copper deposition in the liver biopsy.[5]

Conventional MRI sequences may exhibit abnormal signal intensities in basal ganglia and brain stem in the course of WD. The most common finding reported in patients with

[1]Pediatric Radiology, Faculty of Medicine, Erciyes University, Kayseri, Turkey
[2]Biomedical Imaging Research Center, Erciyes University, Melikgazi, Kayseri 38039, Turkey
[3]Pediatric Neurology, Faculty of Medicine, Erciyes University, Kayseri, Turkey
[4]Pediatric Gastroenterology, Faculty of Medicine, Erciyes University, Kayseri, Turkey
[5]Radiology Department, Faculty of Medicine, Bozok University, Yozgat, Turkey
*Corresponding author, Phone: +90-352-207-6666,
E-mail: kzgumus@gmail.com

Received: December 19, 2016 | Accepted: March 29, 2017

WD is the hyperintensity of globus pallidus, striatum, and brain stem on T_2-weighted images that well correlates with the neurologic symptoms.[6–9] Conversely, the shortening of T_1 relaxation time of bilateral lentiform nuclei may be detected prior to neurologic deterioration and is attributed to hepatic dysfunction rather than copper accumulation of affected brain sites.[8,9]

Quantitative susceptibility mapping (QSM) is a relatively new post-processing technique to create susceptibility maps of the brain and has been reported to be highly effective in differentiation of intracranial calcification and hemorrhage.[10–15] It was also utilized in quantification of iron levels in the human brain.[16] A recent study has shown that copper (II) compounds could result in a measurable difference in susceptibility maps in patients with WD compared to healthy controls at magnetic field strength of 7 Tesla.[17] To the best of our knowledge, this study was the first and only study that focuses on the quantification of the copper accumulation in the basal ganglia with the implementation of QSM technique.

In the current study, we hypothesized that susceptibility changes throughout the basal ganglia and brain stem of patients with neurological WD could be detected prior to any alterations on T_1- and T_2-weighted MRI images using QSM method. We aimed to quantitatively measure the susceptibility changes of basal ganglia and brain stem in patients with WD using QSM technique obtained from a 1.5 Tesla clinical scanner.

Methods

Patient selection

Sixty five patients that were being followed up with the diagnosis of WD by the pediatric gastroenterology and neurology clinics of our institution were recruited in this institutional review board approved the study. All patients had either symptomatic or asymptomatic liver involvement. The diagnosis of WD was based on combinations of presence of Kayser-Flesher ring detected with slit lamp examination, increased urinary copper excretion, decreased serum ceruloplasmin level, and quantification of copper with liver biopsy.[5,18] Patients were evaluated for the presence of any neurologic findings by two pediatric neurologists. Subsequently, 54 patients that had no neuropsychiatric findings (hepatic form) were excluded and 11 patients with neurologic impairment (neurological form) were recruited. The control group consisted of 14 children who came to the pediatric neurology clinic with the symptom of headache but otherwise healthy after the clinical evaluations. The mean age for the patients and the control group were 15 ± 3.3 years (four males, range 10–22 years) and 13.2 ± 2.4 years (six males, range 8–16 years), respectively. The control group had normal levels of serum ceruloplasmin and urinary copper excretion. The subjects and their parents were informed about the study concept and written informed consent was obtained. Two pediatric neurologists who were blinded to cranial MRI findings reviewed the clinical data of the patients in consensus and recorded.

MR Imaging and QSM Analysis

The cranial MRI examinations were obtained on a 1.5T clinical scanner (Magnetom Aera, Siemens, Erlangen, Germany) using a 20-channel neuro coil with the following protocol; a) coronal and axial T_2-weighted turbo spin echo, b) 3D T_1-weighted Magnetization Prepared Rapid Acquisition Gradient Echo (MPRAGE) c) axial 3D multi-echo spoiled gradient echo (GRE) sequence (T_2^*). The protocol parameters for the multi-echo spoiled GRE sequence were as follows: flip angle = 25°, TR = 80 ms, number of echoes = 5, TE = [8.3, 16.8, 24.7, 32.7, 40.7] ms, number of slices = 64, slice thickness (ST) = 2.5 mm, FOV = 220 × 206 mm, Matrix: 192 × 154, bandwidth (BW) = 130 Hz/pixel, GRAPPA acceleration factor of 2, and acquisition time (T_{acq}) = 4 min 17s.

QSM images were reconstructed from multi-echo GRE images. The reconstruction routine involved phase unwrapping, background phase removal using projection onto dipole fields (PDF) approach[18] and morphology-enabled dipole inversion (MEDI)[19,20] to reconstruct the susceptibility maps.

Region of interest analysis was performed on six regions of each hemisphere and two regions of the half of the brain stem: anterior and posterior of globus pallidus, anterior and posterior of putamen, caudate nucleus, thalamus, substantia nigra in the midbrain, and lastly posterior part of the pons adjacent to the cerebral aqueduct on QSM images. ROIs were drawn manually on a single slice where the region of interest is best visible, using ImageJ software[21] by a pediatric radiologist together with an observer radiologist in consensus. Each ROI was delineated according to anatomical boundary of the interested region. An additional measurement was obtained from cerebrospinal fluid (CSF) using a circular ROI inside the fourth ventricle. The CSF measurement value was subtracted from the other measured values for referencing. Two-sample *t*-test was implemented to compare the susceptibility measurements between the patients and controls. A P value <0.05 was considered as significant.

The images of T_1, T_2, and T_2^* sequences of both the patient and the control group were qualitatively evaluated by two pediatric radiologists in consensus for the presence of any signal alterations throughout the basal ganglia and brain stem.

Results

The patients had neurologic symptoms including tremor, dystonia, dizziness, lack of strength, and headache. Kayser-Fleischer rings were detected in five (45%) of the patients. Elevated liver function tests were present in all patients but one, while all patients had clinic and radiologic findings of chronic liver failure. The mean duration of follow up was 48.2 ± 38.1 months and the patients had been treated with D-penicillamine and zinc since the definitive diagnosis was established (Table 1).

Table 1. Features of study patients and magnetic resonance imaging findings

Patient	Gender	Age at diagnosis (year)	Age at MRI acquisition (year)	Duration of follow-up (month)	Time of diagnosis-first neurologic symptom (month)	Presentation with neurologic symptoms	Neurologic symptoms	Kayser-Fleischer ring	Liver biopsy	T_1 hyper intensity	T_2 hyper intensity	T_2* hypo intensity
1	M	13	15	15	–	+	Dystonia, tremor, ataxia	+	+	–	Bilateral P, CN, SN	Bilateral CN, GP, SN, Red nuc.
2	F	7	22	128	108	–	Dystonia, tremor, headache	+	–	Bilateral GP	–	Bilateral CN, GP, SN, Red nuc.
3	F	11	16	45	36	–	Tremor, headache	+	–	–	–	Bilateral GP, SN, Red nuc.
4	F	6	14	82	36	–	Headache, dizziness	–	+	–	–	Bilateral GP, SN, Red nuc.
5	F	8	16	80	72	–	Headache, dizziness, syncope	–	+	–	–	Bilateral GP, SN
6	F	5	12	78	60	–	Headache	–	+	–	–	Bilateral GP, SN
7	M	10	11	16	–	+	Headache, sudden lack of strength	+	+	–	–	Bilateral GP, SN, Red nuc.
8	M	15	17	15	12	–	Tremor	–	+	–	–	Bilateral GP, SN, Red nuc.
9	M	7	10	24	26	–	Headache, dystonia	–	+	–	–	Bilateral GP, SN, Red nuc.
10	F	15	16	18	–	+	Tremor, ataxia, fever, vomiting	+	+	–	–	Bilateral GP, SN, Red nuc.
11	F	10	16	29	18	–	Headache, tremor	–	+	–	–	Bilateral GP, SN, Red nuc.

GP, globus pallidus; CN, caudate nucleus; SN, substantia nigra; P, putamen; Nuc, nucleus.

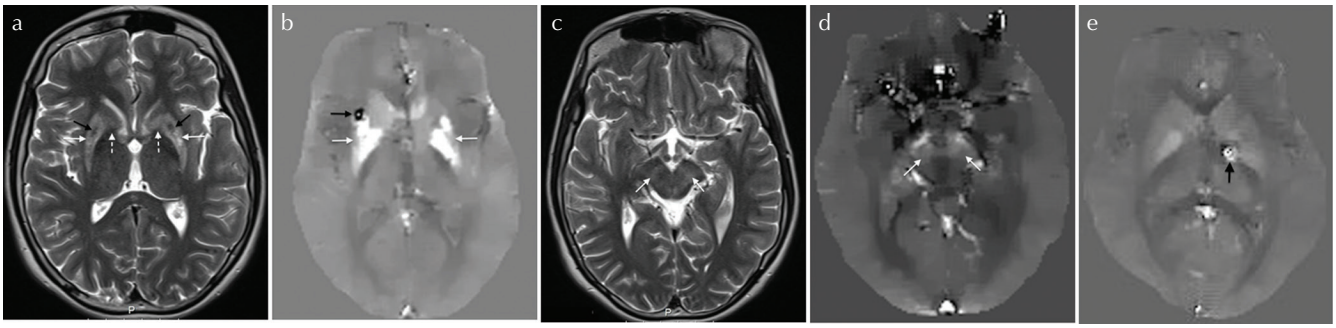

Fig. 1 The MR images of a 15-year-old male with Wilson's disease (WD) revealed (**a**) increased signal intensity of bilateral caudate nuclei (dashed arrows) and putamen (white arrows) on T_2-weighted axial image. Note the central hypointensity of bilateral anterior putamen (black arrows). quantitative susceptibility mapping (QSM) image (**b**) shows the increased susceptibility changes of bilateral globus pallidus and putamen qualitatively (white arrows). The artifact, anterolateral to right putamen is also revealed (black arrow). In addition to basal ganglia involvement, tegmentum in the mesencephalon also has the increased signal on T_2-weighted image (arrows) (**c**). Although not as prominent as in T_2-weighted image, on QSM image (**d**) the increased susceptibility changes of bilateral tegmentum can be appreciated (arrows). QSM image (**e**) of age-matched (15-year-old, male) control patient shows relatively low susceptibility differences of bilateral globus pallidus and putamen. Note the artifact located on left globus pallidus (black arrow).

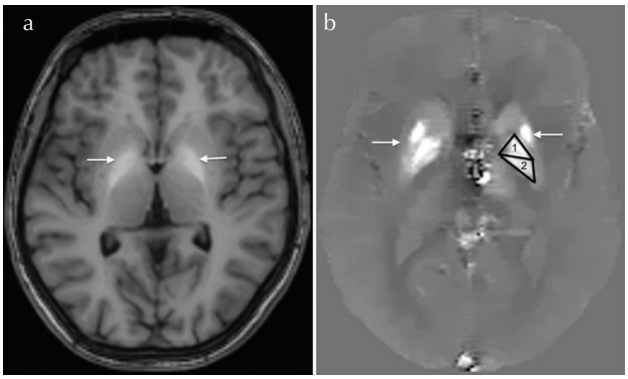

Fig. 2 A 22-year-old female followed up with the diagnosis of Wilson's disease (WD). On T_1-weighted axial MR image (**a**) note the increased signal intensity of bilateral globus pallidus (arrows). quantitative susceptibility mapping (QSM) image (**b**) reveals the increased susceptibility changes qualitatively in bilateral lentiform nucleus (arrows). On left globus pallidus, one and two stand for the ROIs drawn for anterior and posterior parts of globus pallidus, respectively.

When T_1- and T_2-weighted MR images were solely evaluated, two patients with WD were detected to have signal abnormalities on basal ganglia and brain stem: One patient had increased signal intensity on T_2-weighted images involving bilateral symmetrical head of caudate nucleus, putamen, and midbrain. There was no accompanying T_1 shortening (Fig. 1a). On T_1-weighted images of other patient, the bilateral globus pallidus was revealed hyperintense, without any abnormal signal alterations on T_2-weighted images (Fig. 2a). The rest of the patients with WD and the control group did not have any signal changes or structural abnormalities on conventional MR sequences.

The qualitative assessment of T_2^* images of patients with WD revealed reduced signal intensity of bilateral globus pallidus, substantia nigra of all patients. In nine patients, out of 11 (82%) the bilateral red nucleus was hypointense while the bilateral putamen and head of caudate nuclei displayed decreased signal intensity in two different patients (Table 1). In the control group, all patients had reduced signal intensity in the bilateral globus pallidus. The bilateral substantia nigra were detected with decreased signal intensity in 13 patients (13/14 patients, 93%) while the bilateral red nucleus was hypointense in four patients (4/14 patients, 28%).

We observed a signal loss artifact (the black arrow in Fig. 1b) on some QSM images that hindered ROI measurement from globus pallidus and/or putamen in about three subjects in each group. Its possible origin is discussed in the discussion. The susceptibility values between the patient and the control were found to be significantly different in the regions of globus pallidus, putamen, thalamus located on the right hemisphere ($P < 0.05$). The ROI analysis of bilateral caudate nuclei, posterior part of left globus pallidus, anterior part of left putamen, left thalamus did not reveal any significant difference in susceptibility values between the patients and the control group ($P > 0.05$). When brain stem was evaluated, the susceptibility changes of the substantia nigra and pons were more prominent in the patients than the control. However, susceptibility values were not significantly increased in the left substantia nigra ($P = 0.11$). The measured values of QSM maps are presented in Table 2 and Fig. 3.

Discussion

This study evaluates the ability of QSM method to quantify the susceptibility changes in the basal ganglia and brain stem of patients with neurological WD. Our data presents that increased susceptibility changes in the brains of patients with WD compared to the control group could be detected with QSM method prior to any alterations evident on T_1- and T_2-weighted MR images.

Table 2. Susceptibility values of the basal ganglia, thalamus, and brain stem in the patient and the control groups. The susceptibility values were significantly different between patients and controls except left-posterior globus pallidus, left anterior putamen, bilateral caudate nuclei, left thalamus, and left tegmentum

brain regions	Susceptibility values (ppm)		*p* value
	Patients	Control group	
Right-anterior globus pallidus	0.21 ± 0.08	0.15 ± 0.03	0.02
Right-posterior globus pallidus	0.17 ± 0.06	0.13 ± 0.03	0.04
Left-anterior globus pallidus	0.23 ± 0.09	0.15 ± 0.05	0.01
Left-posterior globus pallidus	0.15 ± 0.07	0.13 ± 0.05	0.40
Right-anterior putamen	0.07 ± 0.03	0.04 ± 0.02	0.00
Right-posterior putamen	0.08 ± 0.04	0.04 ± 0.02	0.01
Left-anterior putamen	0.04 ± 0.04	0.04 ± 0.03	0.47
Left-posterior putamen	0.07 ± 0.05	0.04 ± 0.02	0.03
Right caudate nucleus	0.06 ± 0.04	0.06 ± 0.03	0.42
Left caudate nucleus	0.12 ± 0.19	0.07 ± 0.03	0.22
Right thalamus	0.04 ± 0.03	0.01 ± 0.01	0.01
Left thalamus	0.03 ± 0.03	0.02 ± 0.02	0.22
Right tegmentum	0.10 ± 0.06	0.03 ± 0.04	0.00
Left tegmentum	0.10 ± 0.07	0.07 ± 0.04	0.11
Right pons	0.03 ± 0.05	0.08 ± 0.05	0.02
Left pons	0.03 ± 0.05	0.08 ± 0.05	0.01

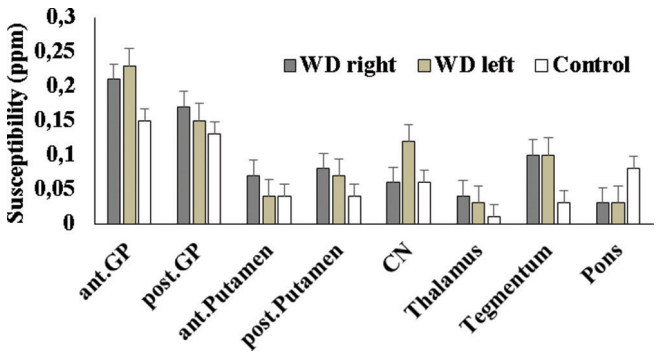

Fig. 3 Susceptibility values in various regions in the right and left brains of the patients with Wilson's disease and the control subjects. GP, Globus Pallidus; CN, Caudate Nucleus; ant, anterior; post, posterior; WD, Wilson's disease.

The pathologic effect of increased extracellular copper is primarily oxidative stress and cell demolishment that particularly affects the brain stem and basal ganglia.[22,23] Ceruloplasmin, in addition to being the main copper carrying plasma protein, catalyzes the conversion of Fe2+ into Fe3+ and plays a crucial role in iron transportation across cell membrane.[24] Ceruloplasmin deficiency may cause brain iron deposition as well as copper (II) and facilitate neuronal degeneration.[25,26] Since both copper (II) and iron are paramagnetic, the susceptibility changes observed in the basal ganglia and brain stem in the patients with WD might be attributable to iron and copper deposition.

Quantitation of minerals such as iron and copper deposited in the human brain is a subject of radiological studies.[27] Copper and copper (I) compounds are diamagnetic like water while copper (II) compounds are paramagnetic. Paramagnetic minerals in tissue alter the phase of local MR signal. The phase shift depends on echo time and perturbation of magnetic field due to susceptibility effects. Susceptibility Weighted Imaging (SWI) relies on phase information to yield a contrast based on local susceptibility differences in the tissue.[28] Depending on the susceptibility differences, SWI has been shown to reveal deep gray nuclei and cerebral cortical mineralization in patients with WD.[29,30] Furthermore, SWI technique may indicate mineral deposition in caudate nuclei, globus pallidus, putamen, thalamus, substantia nigra, and red nucleus based on the phase values in WD.[30–32] With the introduction of QSM technique, it has been possible to map magnetic susceptibility of brain tissue *in vivo*. QSM is a post-processing technique that inverts the phase data to magnetic susceptibility maps.[18–20] Unlike SWI, QSM enables quantitative measurement of tissue susceptibility rather than its effect on the phase data. QSM is a relative technique. The susceptibility value on a region of interest needs to be evaluated to a reference region that was CSF in our analysis. Increased susceptibility value relative to the reference region generally indicates paramagnetic minerals such as iron and copper (II) compounds in the tissues. Magnetic susceptibility of an object is theoretically independent of the static magnetic field.[33] The susceptibility values obtained at 1.5T and 7T must be theoretically same. However, phase contrast increases at high magnetic field strengths. Thus, QSM benefits from the high field strength, resulting in better susceptibility contrast at high tesla.[17] This study demonstrates that QSM images obtained from 1.5T data can be sensitive to the susceptibility changes in the diseased brain.

Previously, putamen has been reported to be the most frequently involved region in the basal ganglia revealing hyperintensity on T_2-weighted MR images followed by the other components of the corpus striatum and thalamus.[2,5–10] However, MRI scans may be completely normal on conventional sequences (T_1- and T_2-weighted) even in the presence of neurological symptoms, which may be related to the duration of the disease and serum copper level.[8] Since our study group consisted of predominantly pediatric patients, all the

patients except two had no signal alterations in the basal ganglia on T_1- and T_2-weighted MR images possibly because of the short duration of the disease. One patient had T_2 prolongation involving bilateral basal ganglia while another one exhibited hyperintensity in bilateral globus pallidus on T_1-weighted MR image. However, QSM images were capable of showing increased susceptibility differences of basal ganglia and thalami in the patients compared to the control group even before the manifestation of signal alterations on T_1- and T_2-weighted images. The susceptibility changes of right entire and left anterior globus pallidus, right entire and left posterior putamen, right thalamus were significantly different between the patients and controls. The distribution of increased susceptibility changes in the basal ganglia of patients with WD is concordant with a recent report of Fritzsch et al.[17] The susceptibility measures of the left anterior putamen, left thalamus and left posterior globus pallidus were not significantly different between the patients and the controls. This could be related to artificial effect due to the artifact on QSM maps.

T_2-weighted MR images may reveal the characteristic 'double panda sign' in WD that points the involved sites of the brain stem: 'Giant panda' is seen in the midbrain and constituted by the hyperintensity of the tegmentum, preservation of signal intensity of the bilateral red nuclei, the lateral part of the substantia nigra and hypointensity of superior colliculus. 'Panda cub' is formed by the hyperintensity of dorsal pons.[34,35] In the current study, solely one patient had aforementioned typical involvement of the midbrain on T_2-weighted MR image. We, for the first time in the literature, compared the susceptibility differences of the brain stem of the patients with WD and healthy controls. The measured susceptibility values of substantia nigra and dorsal pons in the patients exhibited significant increase except the left side of the substantia nigra.

The study has some limitations. Our study group was relatively small since we only focused on the neurologically impaired patients with WD. Therefore, further studies with larger patient groups are needed to test and validate our preliminary results. The scope of the new study to be conducted may be comparing the susceptibility changes of patients with neurologic and hepatic WD at a magnetic strength of 1.5 Tesla. The second limitation is that, our study group predominantly was constituted of pediatric patients and duration of the disease was shorter compared to adult age group. So, a study conducted by recruiting elder patients may result with more significantly increased susceptibility changes. Third, some of our measurements suffered from a signal loss artifact on QSM images. We do not know what caused this artifact and continue to investigate its origin. The artifact was localized in a single place mostly on the left side of the brain. We did not take ROI measurements if it was covering the region of our interest. Lastly, we made ROI measurements on a single slice. Future studies should aim to perform measurements from 3D ROIs.

In conclusion, QSM method may exhibit increased susceptibility differences of basal ganglia and brain stem in patients with neurologic WD prior to the detection of any signal alteration on T_1- and T_2-weighted MR images at a magnetic field strength of 1.5 Tesla. The susceptibility changes might be an early indicator for WD.

Conflicts of Interest

The authors declare that they have no conflicts of interest.

References

1. Ala A, Walker AP, Ashkan K, Dooley JS, Schilsky ML. Wilson's disease. Lancet 2007; 369:397–408.
2. Ferenci P. Wilson's disease. Clin Liver Dis 1998; 2:31–49.
3. Ferenci P, Caca K, Loudianos G, et al. Diagnosis and phenotypic classification of wilson disease. Liver Int 2003; 23:139–142.
4. Nazer H, Brismar J, al-Kawi MZ, Gunasekaran TS, Jorulf KH. Magnetic resonance imaging of the brain in Wilson's disease. Neuroradiology 1993; 35:130–133.
5. European Association for Study of Liver. EASL clinical practice guidelines: Wilson's disease. J Hepatol 2012; 56:671–685.
6. Prayer L, Wimberger D, Kramer J, Grimm G, Oder W, Imhof H. Cranial MRI in Wilson's disease. Neuroradiology 1990; 32:211–214.
7. Sinha S, Taly AB, Ravishankar S, et al. Wilson's disease: cranial MRI observations and clinical correlation. Neuroradiology 2006; 48:613–621.
8. Kim TJ, Kim IO, Kim WS, et al. MR imaging of the brain in Wilson disease of childhood: findings before and after treatment with clinical correlation. AJNR Am J Neuroradiol 2006; 27:1373–1378.
9. Roh JK, Lee TG, Wie BA, Lee SB, Park SH, Chang KH. Initial and follow-up brain MRI findings and correlation with the clinical course in Wilson's disease. Neurology 1994; 44:1064–1068.
10. Saatci I, Topcu M, Baltaoglu FF, et al. Cranial MR findings in Wilson's disease. Acta Radiol 1997; 38:250–258.
11. Schweser F, Deistung A, Lehr BW, Reichenbach JR. Differentiation between diamagnetic and paramagnetic cerebral lesions based on magnetic susceptibility mapping. Med Phys 2010; 37:5165–5178.
12. Liu C, Li W, Tong KA, Yeom KW, Kuzminski S. Susceptibility-weighted imaging and quantitative susceptibility mapping in the brain. J Magn Reson Imaging 2015; 42:23–41.
13. Gumus K. Reconstruction of quantitative susceptibility maps. Radiology 2015; 275:617–618.
14. Chen W, Zhu W, Kovanlikaya I, et al. Intracranial calcifications and hemorrhages: characterization with quantitative susceptibility mapping. Radiology 2014; 270:496–505.
15. Gumus K, Koc G, Doganay S, et al. Susceptibility-based differentiation of intracranial calcification and hemorrhage in pediatric patients. J Child Neurol 2015; 30:1029–1036.

16. Bilgic B, Pfefferbaum A, Rohlfing T, Sullivan EV, Adalsteinsson E. MRI estimates of brain iron concentration in normal aging using quantitative susceptibility mapping. Neuroimage 2012; 59:2625–2635.
17. Fritzsch D, Reiss-Zimmermann M, Trampel R, Turner R, Hoffmann KT, Schäfer A. Seven-tesla magnetic resonance imaging in Wilson disease using quantitative susceptibility mapping for measurement of copper accumulation. Invest Radiol 2014; 49:299–306.
18. Liu T, Khalidov I, de Rochefort L, et al. A novel background field removal method for MRI using projection onto dipole fields (PDF). NMR Biomed 2011; 24:1129–1136.
19. Liu J, Liu T, de Rochefort L, et al. Morphology enabled dipole inversion for quantitative susceptibility mapping using structural consistency between the magnitude image and the susceptibility map. Neuroimage 2012; 59:2560–2568.
20. Liu T, Liu J, de Rochefort L, et al. Morphology enabled dipole inversion (MEDI) from a single-angle acquisition: comparison with COSMOS in human brain imaging. Magn Reson Med 2011; 66:777–783.
21. Schneider CA, Rasband WS, Eliceiri KW. NIH Image to ImageJ: 25 years of image analysis. Nat Methods 2012; 9:671–675.
22. Ferenci P. Pathophysiology and clinical features of Wilson disease. Metab Brain Dis 2004; 19:229–239.
23. Watt NT, Hooper NM. The response of neurones and glial cells to elevated copper. Brain Res Bull 2001; 55:219–224.
24. Sargent PJ, Farnaud S, Evans RW. Structure/function overview of proteins involved in iron storage and transport. Curr Med Chem 2005; 12:2683–2693.
25. Haacke EM, Cheng NY, House MJ, et al. Imaging iron stores in the brain using magnetic resonance imaging. Magn Reson Imaging 2005; 23:1–25.
26. Shiono Y, Wakusawa S, Hayashi H, et al. Iron accumulation in the liver of male patients with Wilson's disease. Am J Gastroenterol 2001; 96:3147–3151.
27. Valdés Hernández Mdel C, Maconick LC, Tan EM, Wardlaw JM. Identification of mineral deposits in the brain on radiological images: a systematic review. Eur Radiol 2012; 22:2371–2381.
28. Haacke EM, Xu Y, Cheng YC, Reichenbach JR. Susceptibility weighted imaging (SWI). Magn Reson Med 2004; 52: 612–618.
29. Skowrońska M, Litwin T, Dziełyc K, Wierzchowska A, Członkowska A. Does brain degeneration in Wilson disease involve not only copper but also iron accumulation? Neurol Neurochir Pol 2013; 47:542–546.
30. Bai X, Wang G, Wu L, et al. Deep-gray nuclei susceptibility-weighted imaging filtered phase shift in patients with Wilson's disease. Pediatr Res 2014; 75:436–442.
31. Yang J, Li X, Yang R, et al. Susceptibility-weighted imaging manifestations in the brain of Wilson's disease patients. PLoS ONE 2015; 10:e0125100.
32. Zhou XX, Qin HL, Li XH, et al. Characterizing brain mineral deposition in patients with Wilson disease using susceptibility-weighted imaging. Neurol India 2014; 62:362–366.
33. Hinoda T, Fushimi Y, Okada T, et al. Quantitative susceptibility mapping at 3T and 1.5 T: evaluation of consistency and reproducibility. Invest Radiol 2015; 50:522–530.
34. Hitoshi S, Iwata M, Yoshikawa K. Mid-brain pathology of Wilson's disease: MRI analysis of three cases. J Neurol Neurosurg Psychiatr 1991; 54:624–626.
35. Jacobs DA, Markowitz CE, Liebeskind DS, Galetta SL. The "double panda sign" in Wilson's disease. Neurology 2003; 61:969.